Vertical profile of atmospheric dimethyl sulfide in the Arctic Spring and Summer

Roghayeh Ghahremaninezhad[1], Ann-Lise Norman[1], Betty Croft[2], Randall V. Martin[2], Jeffrey R. Pierce[3], Julia Burkart[4], Ofelia Rempillo[1], Heiko Bozem[5], Daniel Kunkel[5], Jennie L. Thomas[6], Amir A. Aliabadi[7], Gregory R. Wentworth[4], Maurice Levasseur[8], Ralf M. Staebler[9], Sangeeta Sharma[9] and W. Richard Leaitch[9]

[1] Department of Physics and Astronomy, University of Calgary, Calgary, Canada

[2] Department of Physics and Atmospheric Science, Dalhousie University, Halifax, Canada

[3] Department of Atmospheric Science, Colorado State University, Fort Collins, USA

[4] Department of Chemistry, University of Toronto, Toronto, Canada

[5] Institute of Atmospheric Physics, University of Mainz, Mainz, Germany

[6] Sorbonne Universités, UPMC Univ. Paris 06, Universite Versailles St-Quentin, CNRS/INSU, UMR8190, LATMOS-IPSL, Paris, France

[7] Environmental Engineering Program, School of Engineering, University of Guelph, Guelph, Canada

[8] Department of Biology, Laval University, Quebec, Canada

[9] Environment and Climate Change Canada, Toronto, Canada

Corresponding author: Ann-Lise Norman (alnorman@ucalgary.ca)

Abstract

Vertical distributions of atmospheric dimethyl sulfide (DMS(g)) were sampled aboard the research aircraft Polar 6 near Lancaster Sound, Nunavut, Canada in July 2014 and on pan-Arctic flights in April 2015 that started from Longyearbyen, Spitzbergen, and passed through Alert and Eureka, Nunavut and Inuvik, Northwest Territories. Larger mean DMS(g) mixing ratios were present during April 2015 (campaign-mean of 116±8 pptv) compared to July 2014 (campaign-mean of 20±6 pptv). During July, 2014, the largest mixing ratios were found near the surface over the ice-edge and open water. DMS(g)

mixing ratios decreased with altitude up to about 3 km. During April, 2015, profiles of DMS(g) were more uniform with height and some profiles showed an increase with altitude. DMS reached as high as 100 pptv near 2500 m.

Relative to the observation averages, GEOS-Chem chemical-transport model simulations were higher during July and lower during April. Based on the simulations, more than 90% of the July DMS(g) below 2 km and more than 90% of the April DMS(g) originated from Arctic seawater (north of 66°N). During April, 60% of the DMS(g), between 500 m and 3000 m originated from Arctic seawater. During July, 2014, FLEXPART simulations locate the sampled air mass over Baffin Bay and the Canadian Arctic Archipelago four days back from the observations. During April, 2015, the locations of the air masses four-days back from sampling were varied: Baffin Bay/Canadian Archipelago, the Arctic Ocean, Greenland and the Pacific Ocean. Our results highlight the role of open water below the flight as the source of DMS(g) during July 2014, and the influence of LRT of DMS(g) from further afield in the Arctic above 2500 m during April 2015.

1 Introduction

The Arctic has experienced rapid climate change in recent decades (IPCC, 2013). Its high climate sensitivity distinguishes the Arctic from the rest of the world. The Arctic Ocean moderates Arctic climate and has variable surface temperature and salinity as ice cover melts and freezes (Bourgain et al., 2013). This ocean is an important source of atmospheric gases and particles (e.g. dimethyl sulfide, as well as sea salt, organic and biogenic particles) (e.g. Bates et al., 1987; Andreae, 1990; Yin et al., 1990; Leck and Bigg, 2005a, b; Barnes et al., 2006; Ayers and Cainey, 2007; Sharma et al. 2012). Aerosols affect the climate by scattering/reflecting sunlight (direct effects), changing number/size of cloud droplets and altering precipitation efficiency (indirect effects) (Twomey, 1974; Albrecht, 1989). Shupe et al., (2013) provided the evidence for the formation of clouds and transport of moisture and aerosol particles, likely accompanied warm air masses, from lower latitudes into the central Arctic during summer. The study of these particles has been of interest for numerous researchers because of their importance in Arctic climate change. Najafi et al. (2015) estimated that the net effect of aerosol is cooling the Arctic. However, there

are many uncertainties related to the estimation of effects and sources of aerosol particles. In this study, we focus on one of those sources, DMS(g).

Atmospheric oxidation of DMS(g) is the main source of biogenic sulfate aerosols in the Arctic (Norman et al., 1999). DMS(aq) is produced by the breakdown of dimethylsulfonopropionate (DMSP) by oceanic phytoplankton and bacteria DMSP-lyases (Levasseur, 2013) and transported to the atmosphere via turbulence, diffusion and advection (Lunden et al., 2010). Sulfur compounds from atmospheric DMS(g) oxidation are able to form new particles and condense on pre-existing aerosols in the atmosphere (Chang et al., 2011). If sufficient condensable vapours are available, the particles may grow large enough to act as cloud condensation nuclei (CCN), and Charlson et al. (1987) hypothesized that DMS could provide a negative feedback to stabilize the global warming (CLAW hypothesis). Although no evidence in support of the hypothesis has been found (Quinn and Bates, 2011), DMS(g) emissions may play an important role in the climate of remote areas with low aerosol concentrations, such as in the Arctic (Carslaw et al., 2013, Leaitch et al., 2013, Levasseur 2013, Croft et al., 2016a).

Dimethyl sulfide production and emission to the atmosphere vary seasonally. Production and emission are particularly strong during the Arctic summer time due to high temperature, biological activity, and the amount of ice-free surface area. Melting ice in the marginal ice zone, ice-edge and under-ice are favourable for the production of DMSP and aqueous DMS(aq) by oceanic phytoplankton (Leck and Persson, 1996; Matrai and Vernet, 1997; Levasseur 2013). After summer, aqueous phase DMS(aq) concentrations decrease by about three orders of magnitude between August and October in the central Arctic Ocean (Leck and Persson, 1996).

Dimethyl sulfide oxidation in the atmosphere occurs by the radical addition pathway (by hydroxyl radicals OH and halogen oxides) and by the H abstraction pathway (by the nitrate radical NO_3, OH and halogens) (Barnes et al., 2006; von Glasow and Crutzen, 2004). In general, the DMS(g) oxidation rate and pathway depends on the available oxidants and temperature. The final products of DMS(g) oxidation by the addition pathway are DMSO and MSA. DMSO oxidizes in cloud droplets to meathanesulphonicacid, due to its high solubility and MSA likely condenses onto pre-existing aerosols (von Glasow and Crutzen, 2004). On the other hand, DMS(g) oxidation by the abstraction pathway leads to formation of SO_2. Some of SO_2 removes from the atmosphere via dry and wet deposition and the remaining SO_2 may form sulfuric

acid (H_2SO_4) in the gas and aqueous phases (Pierce et al., 2013). Sulfuric acid formed in the gas phase is a key atmospheric nucleation component which is able to form new particles that may grow to the size of CCN and affect climate (Kulmala et al., 2004).

Previous measurements of DMS(g) in the Arctic atmosphere are limited to a few studies and field campaigns at different locations (e.g. Sharma et al., 1999; Rempillo et al., 2011; Mungall et al., 2016). The study of the vertical distribution of DMS (g) in the Arctic atmosphere is also limited to a few observations. Ferek et al., (1995) reported the first measurements of DMS(g) vertical profiles over the Arctic Ocean near Barrow in early summer 1990 and spring 1992. They reported low DMS(g) mixing ratios (a few pptv) during spring and relatively high (a few tens pptv with some peaks around 100 to 300 pptv) during summer. They concluded that the Arctic Ocean is the potential source of DMS(g), and DMS (g) ocean-atmosphere exchange is more important early summer due to sea ice melt.

Observations of the NASA DC-8 during ARCTAS (https://www-air.larc.nasa.gov/cgibin/ ArcView/arctas) showed low DMS mixing ratios in spring (below detection limit to a few pptv in the boundary layer and a maximum of 1 pptv in the free troposphere) (Simpson et al., 2010; Lathem et al., 2013).

Kupiszewski et al. (2013) measured atmospheric DMS(g) on board a helicopter and observed large variability in DMS(g) mixing ratios over the central Arctic Ocean during summer. The median (mean) values were around 7 (34) pptv near the surface < 200 m, 11 (22) pptv for altitudes between 200 and 1000 m, and 4 (5) pptv above 1000 m.

Lunden et al. (2010) presented model results for the vertical distribution of DMS(g) in the Arctic (north of 70ºN) during summer. They reported a variable vertical profile for DMS(g) concentrations above open water, with the highest concentrations near the surface (around 115 and 365 pptv for the median and 95th percentiles respectively) and an exponential decrease with height. In contrast, over the pack-ice, DMS(g) concentrations were higher above the local boundary layer than at the surface. Also, Lunden et al. (2010) showed that DMS(g) can be mixed downward by turbulence into the local boundary layer and to provide a DMS source over the pack-ice. In addition, they compared modeling results with measurements from the Arctic Ocean Expedition 2001 (AOE-2001, Leck et al., 2004; Tjernström et al., 2004) and reported that DMS(g) was present above the local boundary layer in both the model and observations.

For our study, atmospheric DMS(g) samples were collected onto Tenax tubes during Polar 6 aircraft flights in the Arctic. We compared these DMS(g) measurements to GEOS-Chem chemical transport model simulations and conducted sensitivity simulations to examine the local versus long range transport (LRT) DMS(g) sources for both the spring and summer. In addition, FLEXPART was applied in back trajectory mode in order to investigate the DMS(g) source regions based on potential emission sensitivity simulations. Field and sampling locations, as well as measurement/modeling methods are described in section 2. Section 3 includes DMS(g) measurement data. Section 4 presents discussion of results, and comparison of measurement with modeling results (GEOS-Chem and FLEXPART) are in section 5. The summary and conclusion of this study are reported in section 6.

2 Field description and methods

2.1 Measurements

2.1.1 DMS

DMS(g) was collected aboard the research aircraft Polar 6 in the Arctic during July 2014 and April 2015, as part of the NETCARE (Network on Climate and Aerosols: Addressing Key Uncertainties in Remote Canadian Environments) project. The Polar 6 aircraft routes and sampling locations from 12 to 21 July 2014, and from 5 to 20 April 2015 are shown in Figures 1 and 2, respectively. The Polar 6 campaign was based from Resolute Bay, Nunavut, and covered the Lancaster Sound area in July 2014. In April 2015, the flights started from Longyearbyen, Spitzbergen, and passed through Alert and Eureka, Nunavut and Inuvik, Northwest Territories. DMS sampling locations, altitude, latitude and longitude, are reported in Table 1.

Atmospheric DMS(g) was collected on cartridges packed with Tenax TA®. Mass flow was controlled at approximately 200 ± 20 mL/min, and a KI-treated 47 mm quartz Whatman filter was fitted at the intake of cartridge to remove all oxidants. Two Teflon valves were placed before and after the Tenax tube to control the sampling period, and Teflon tubing was used to transfer the sample from outside the aircraft to the sampler. The samples were stored in an insulated container with a freezer pack after collection and

in a freezer after the flight. Sampling collection time was 300 ± 5 seconds with a flow rate of 200 ± 20 mL/min (for few samples the sampling time was shorter or longer than 300 seconds, leading to different volume of samples).

A glass gas chromatograph (GC) inlet liner was used to pack 170 ± 2 mg of Tenax. The Tenax packed in glass tubes was cleaned by heating to 200˚C in an oven with a constant He flow of around 15 mL/min for 5 hours. The DMS samples were analyzed with using a Hewlett Packard 5890 gas chromatograph (GC) fitted with a Sievers Model 355 sulfur chemiluminescence detector (SCD). Two DMS(g) certified standards (1 and 50 ppmv) were used to calibrate the GC-SCD and to determine accuracy of the measurements by checking the standards against each other (for example, 1 microliter of 50 ppmv vs 50 microliters of 1 ppmv). Collection and analysis of samples were based on methods described by Sharma (1997), Sharma et al. (1999) and Rempillo et al. (2011). Uncertainty in the measurements was determined based on the standard deviation (σ) of DMS(g) standards and was ±12 pptv. The detection limit for this method is approximately 7 pptv.

Additional tests were performed to determine if there was significant loss of DMS(g) over time after collection. An experiment was performed to determine how long Tenax is able to store DMS(g) with no significant loss of concentration. This experiment was conducted in triplicate by loading of 50 µL of 1 ppmv DMS(g) standard and storing in a freezer at -25˚C. In general, Tenax storage tests at -25˚C showed that DMS losses were approximately 5% and 15% after 10 and 20 days respectively (Figure 3). The DMS(g) mixing ratios summarized in Table 1 are adjusted according to the result of this test.

2.1.2 Meteorological measurements

Meteorological measurements were performed by an AIMMS-20 (Aircraft Integrated Meteorological Measurement System) instrument, manufactured by Aventech Research Inc., Barrie, Ontario, Canada. This instrument was used to measure the three-dimensional, aircraft-relative flow vector (true air speed, angle-of-attack, and sideslip), temperature, relative humidity, turbulence, and horizontal/vertical wind speeds. Accuracy and resolution were 0.30 and 0.01 ˚C, respectively for temperature and 2.0 and 0.1 % respectively for relative humidity. More details of the instrument and corresponding aircraft

measurements were recently published in other studies from the same campaign (e.g. Leaitch et al., 2016, Aliabadi et al., 2016b, and Willis et al., 2016).

2.2 Model Description

2.2.1 GEOS-Chem Chemical Transport Model

The GEOS-Chem chemical transport model (www.geos-chem.org) was used to interpret the vertical profile of DMS(g). We used GEOS-Chem version 9-02 at 2×2.5º resolution with 47 vertical layers between the surface and 0.01 hPa. The assimilated meteorology is taken from the National Aeronautics and Space Administration (NASA) Global Modeling and Assimilation Office (GMAO) Goddard Earth Observing System version 5.7.2 (GEOS-FP) assimilated meteorology product, which includes both hourly surface fields and 3-hourly 3D fields. Our simulations used 2014 and 2015 meteorology following a 1-month spin-up prior to the simulation of July 2014 and April 2015.

The GEOS-Chem model includes a detailed oxidant-aerosol tropospheric chemistry mechanism as originally described by Bey et al. (2001). DMS(g) emissions are based on the Liss and Merlivat (1986) sea-air flux formulation, and oceanic DMS(g) concentrations from Lana et al. (2011). In our simulations, DMS(g) emissions occurred only in the fraction of the grid box that is covered by seawater and also free of sea ice. Simulated DMS(g) oxidation occurs by reaction with OH and NO_3. The model also includes natural and anthropogenic sources of SO_2 and NH_3 (Fisher et al. 2011). Oxidation of SO_2 occurs in clouds by reaction with H_2O_2 and O_3 and in the gas phase with OH (Alexander et al, 2009). Reaction rates and the yields of SO_2 and MSA from DMS(g) oxidation are determined by DeMore et al. (1997) and Chatfield and Crutzen (1990), respectively. The simulated aerosol species include sulfate-nitrate-ammonium (Park et al. 2004; 2006), carbonaceous aerosols (Park et al, 2003; Liao et al. 2007), dust (Fairlie et al. 2007; 2010) and sea salt (Alexander et al. 2005). The sulfate-nitrate-ammonium chemistry uses the ISORROPIA II thermodynamic model (Fountoukis et al. 2007), which partitions ammonia and nitric acid between the gas and aerosol phases. Climatological biomass burning emissions are from the Global Fire Emissions Dataset (GFED3).

The GEOS-Chem model has been extensively applied to study the Arctic atmosphere, in regard to aerosol acidity (Wentworth et al., 2016; Fisher et al., 2011) carbonaceous aerosol (Wang et al., 2011), aerosol number (Leaitch et al., 2013, Croft et al., 2016a, b), aerosol absorption (Breider et al., 2014), mercury (Fisher et al. 2012), and recently surface-layer DMS(g) (Mungall et al. 2016).

2.2.2 FLEXPART-ECMWF

For this study, the Lagrangian particle distribution model, FLEXPART model (Stohl et al., 2005; website: https://www.flexpart.eu/) is driven by global meteorological analysis data from European center for medium-range weather forecasts (ECMWF) for July 2014 and April 2015. For the ECMWF data a horizontal grid spacing of 0.25° was used along with 137 hybrid sigma-pressure levels in the vertical from the surface up to 0.01 hPa. FLEXPART was operated in backward mode to estimate potential emission sources and transport pathways influencing Polar 6 DMS(g) measurements in summer 2014 and spring 2015. For this plumes of a passive tracer with properties of air, i.e., molar mass of dry air, no removal, were released along the flight paths every minute. These plumes were traced back for several days to study the potential origin of the air masses sampled during the flights with the Polar 6.

3 DMS measurement and discussion

DMS(g) concentrations as a function of altitude are shown in Figure 4 for the July 2014 and April 2015 flights. The campaign-mean DMS(g) mixing ratios were 20±6 pptv (maximum of 114 pptv) for July 2014 and 116±8 pptv (maximum of 157 pptv) for April 2015.

The 2014 sampling locations focused on the Lancaster Sound, Nunavut region in July 2014, whereas sampling in April 2015 occurred over a broad region of the Arctic: Longyearbyen, Spitzbergen, Alert and Eureka, Nunavut and Inuvik, Northwest Territories. Observations on individual flights in July 2014 indicate either decreasing DMS(g) mixing ratios with increasing altitude or relatively uniform DMS(g) mixing ratios (independent of altitude below 3 km). During spring of the following year (April 2015), DMS(g) mixing ratios on individual flights were more uniform with altitude below 4 km and in some cases increased with altitude.

Figure S1 shows the ice fraction for July 2014 flights. During July, 2014, the highest DMS(g) mixing ratios were measured near ice-edges and above open waters (e.g. samples >40 pptv, July 12, 20 and 21). That, and the decrease of atmospheric DMS(g) with altitude, suggest the atmospheric DMS(g) was locally sourced (Lancaster Sound and Baffin Bay) during the month of July, consistent with the findings of Mungall et al. (2016) conducted from the icebreaker CCGS Amundsen. Mungall et al. (2016) also suggested LRT of DMS from marine regions outside Baffin Bay and Lancaster Sound area, and observed an episode of elevated DMS (g) mixing ratios with values of 400 pptv or above occurred on 18–20 of July. The airborne measurement, showed decline of DMS (g) mixing ratios by height during July 17, and relatively low DMS mixing ratios during July 19th and 20th (see Table 1). The decline in DMS(g) mixing ratios with height may be due to a combination of weak vertical mixing and photochemical reactions.

Previous observations of seasonal variations in DMS(aq) in the Arctic Ocean found the maximum DMS(aq) occurred in July and August (e. g. Bates et al., 1987; Leck and Persson, 1996, Levasseur 2013). After the August peak, DMS(aq) declines due to lower biological activity (Leck and Persson, 1996). From DMS concentrations in both the surface ocean and in the atmosphere just above the ocean surface (median DMS (g) of 186 pptv), Mungall et al. (2016) estimated the air-sea DMS(g) flux ranging from 0.02–12 μmol m^{-2} d^{-1} in July 2014 in the same location as the present measurements (Lancaster Sound). For the same campaign, Ghahremaninezhad et al. (2016) showed that the dominant source for fine aerosol and SO_2 measured onboard the Amundsen at the same location and about 30 m above the ocean's surface was biogenic sulfur, arising from DMS(g) oxidation. Atmospheric oxidation of DMS(g) is expected to proceed more readily in the summertime Arctic atmosphere than in spring, due to higher temperatures and more sunlight. However, relatively high DMS mixing ratios (> 15 pptv) were observed for July 12th at high altitudes (> 800 m), and FLEXPART results shows influence of local source, Lancaster Sound for that day (mentioned in Section 4.2). On this day, NETCARE results do not follow the usual DMS vertical pattern of high DMS at the surface declining with altitude to near zero above the MBL. Instead, high concentrations aloft on July 12 imply convective transport into the free troposphere and potentially an extended photochemical lifetime due to reduced water vapor or limited sunlight.

During April, DMS(g) samples were collected above ice and snow surfaces, and heat fluxes were negligible. Figure S3 shows the ice fraction during the April 2015 campaign. The higher DMS(g) mixing

ratios in April, in the free troposphere over ice-covered regions (Figure 4, right panel), stability of the Arctic atmosphere, and limited vertical mixing, suggest that DMS(g) can be transported to the sampling locations from other regions within the Arctic and/or from lower latitudes (except for April 4 when DMS(g) sampling was above open water). These results contrast with results from Ferek et al., (1995) where lower DMS(g) mixing ratios (a few pptv) were found over the Arctic Ocean near Barrow during spring 1992. Andrea et al. (1988) presented vertical profiles of DMS(g) mixing ratios measured over the northeast Pacific Ocean during May 1985 (with a maximum ~ 30 pptv in the mixed layer and also 3600 m). They found that DMS(g) mixing ratios depend on the stability of the atmosphere and air mass sources and that long-range transport at mid tropospheric levels was important in remote areas of the northern hemisphere.

The relatively larger observed DMS(g) away from open water sources springtime relative to summer suggests longer DMS(g) lifetimes in April than July, possibly due to lower OH mixing ratios enabling more long-range range transport of DMS(g) (Li et al., 1993). Lower water vapour and higher DMS mixing ratios during the spring compared with the summer (Fig. S2) suggests that more of the April DMS(g) originated from open water sources further away from the observations point than in summertime. The greater ice cover and increased presence of DMS(g) at higher altitudes during April suggests an origin from further south than in summertime. More water vapour will initially accompany that DMS(g), but the Arctic is cold in April, especially aloft, and the low water vapour indicates significant loss via cloud processes during transport. Some of the water vapour loss will occur via the ice phase, and DMS oxidation in the aqueous-phase was likely relatively insignificant during this time (Henry's Law constant for DMS is relatively small: 0.14 mol/L-atm) or the DMS(g) values at their origin were much higher than the present observations.

Ozone depletion during spring was observed within the boundary layer (Fig S2) and is well documented in the literature (e.g. Barrie et al., 1989). Ozone depletion may further decrease OH near the surface and enhance DMS(g) lifetimes in the boundary layer due to reduced oxidation rates, contributing to the relatively larger springtime DMS(g) in our measurements. However, if DMS is present in the ozone-

depleted boundary layer, halogen oxides, such as BrO radical, can be more important during winter/spring than summer and could oxidize DMS(g) (von Glasow et al., 2004, Chen et al., 2016).

DMS (g) vertical profiles are sensitive to the boundary layer height. For the summertime, Arctic the boundary layer height on various days (275±164 m), for the July 2014 campaign, is reported in Aliabadi et al. (2016). They showed that the profiles of the potential temperature exhibited a positive vertical gradient throughout the aircraft campaign (their Fig. 4). In addition, using vertical profiles of wind speed, they derived a positive gradient Richardson number (Ri) with a median of 2.5 (Their Fig. 7) throughout the aircraft campaign. The magnitude of the positive gradient Richardson number is an indicator of the strength of thermal stability in the atmospheric boundary layer. Due to the strong thermally stable conditions during the field campaign, mixing was weaker compared to well-mixed boundary layers at mid latitudes. As a result the summertime measurements show a strong decrease in DMS(g) above the boundary layer. Although there is no reference for the April 2015 campaign boundary layer, we expect similar boundary layer characteristics in the stable Arctic boundary layer at high latitudes due to the even more reduced thermal forcing with large sun angles in the month of April compared to the month of July. The springtime measurements show a more uniform vertical profile suggesting transport in the free troposphere from open water sources that were relatively farther distance from the observation point in springtime than in summer.

Aerosol number concentrations and size distributions during the July, 2014 study are discussed by Willis et al. (2016) and Burkart et al. (2017), who show that increases in the number concentrations of smaller particles (5-20 nm), believed to reflect new particle formation (NPF), occurred principally near the surface during July 12th 2014. The highest levels of DMS(g) during the July study also occurred near the surface (Fig. 4a), and both Willis et al (2016) and Burkart et al. (2017) noted increased MSA near the surface associated with two case studies of NPF. In the clean conditions of the Arctic summer (e.g. CO in Fig. S2), the low-level DMS may contribute to NPF. The springtime Arctic differs in that the aerosol mass near the surface is much higher, resulting in a higher condensation sink that, in addition to other potential factors, inhibits NPF. During the springtime flights, there was no evidence for NPF near the surface, and

only a few instances aloft. Unfortunately, no sampling for DMS coincided with those few events, and we cannot say if they were connected with the DMS(g) aloft.

4 Chemical-transport-model simulations and discussion

4.1 GEOS-Chem

We simulated the vertical profile of DMS(g) mixing ratios with the GEOS-Chem chemical-transport model, and the model was co-sampled along the Polar 6 aircraft tracks. Recently, GEOS-Chem was used to interpret DMS(g) measurements in the Arctic surface-layer atmosphere (Mungall et al., 2016). However, despite the significant influence of DMS(g) on the Arctic climate relative to lower latitudes and the importance of where DMS(g) oxidation occurs vertically (Woodhouse et al., 2013), measurements of DMS(g) vertical profiles are rare in the Arctic atmosphere.

Figure 5 shows the campaign-mean vertical profile of DMS(g) for the co-sampled GEOS-Chem simulation and our measurements for both July 2014 and April 2015. Caution should be used in interpreting the model-measurement comparisons since these comparisons are conducted over a very limited number of measurement periods and the spatial and temporal resolution of these measurements is a challenge for a global model to simulate. In July 2014, both the measurements and simulation show a strong decrease of DMS(g) mixing ratios with altitude in the lowest 300 m. Aliabadi et al. (2016a and 2016b) estimated the boundary layer height as 275±164 m, using data from radiosondes launched at Resolute Bay and the Amundsen icebreaker, during the 2014 campaign. Aliabadi et al. (2016b) indicated that the magnitude of turbulent fluxes of momentum, heat and the associated diffusion coefficients are significantly reduced above the boundary layer height during the 2014 campaign. Thus, we find the strongest vertical gradient between the boundary layer and above. In the boundary layer, the GEOS-Chem simulation over predicts the measurements, but is within a factor of 2 to 3. Hoffman et al. (2016) showed that DMS chemistry should be considered in the aqueous phase as well as the gas-phase to improve modeling predictions. This chemistry is not included in our model could contribute to model's over prediction of the measurements at these lower altitudes. Above 1500 m, the simulation under predicts the measurements. Overall, the simulations and observations agree within their respective variabilities.

The April 2015 campaign-mean shows a more gradual decrease with altitude (Figure 5, right panel). As well, mixing ratios are greater than during the July campaign. Both the simulated and measured DMS(g) profiles during spring (~ 30 to >50 pptv) show more variability at all altitude below 4 km than in summer (~ 20 to 40 pptv at low altitudes and <10 pptv at higher altitudes). Ozone depletion not represented by the simulation is one potential explanation for the underestimated DMS(g) in the simulations since the oxidation rates may be too high. Surface layers depleted of ozone were observed on several occasions during April 2015: 3 of 5 samples collected at 60 m above ice surfaces were concurrent with measured ozone depletion events (<1 ppbv) during the April campaign (shown in Table 1). If the DMS(g) oxidation potential is reduced by ozone depletion the lifetime of DMS(g) in the region of ozone depletion may increase. Another reason for underestimation by the model may be errors in the simulated source strength. The monthly mean seawater DMS field used in our simulations is based on very limited observations from this region (Lana et al., 2011). Datasets of seawater DMS with higher spatial and temporal resolution are needed but are still under development.

We conducted a sensitivity simulation to identify the latitude-dependent contribution of the oceans to the simulated DMS(g) at the sampling points along the flight tracks. In Figure 5, the "SimZeroBelow66" simulation has no ocean DMS(g) for all latitudes south of 66°N. This simulation compared with the standard simulation suggests that a large majority of the campaign-mean DMS(g) for both April and July arises from the oceans north of 66°N.

As given in Table 2, the 'SimZeroBelow66' simulates 97% or more of the DMS(g) below 500 m during July coming from waters north of 66°N. The fractional contribution from north of 66° is about 90% for April and at the same altitudes; although different regions were sampled at that time. The simulations attribute about 60% and 90% of the DMS(g) at altitudes from 500-3000 m to seawater north of 66°N in April and July, respectively. This 30% difference indicates a greater contribution from long-range transport from lower latitudes in the springtime.

4.2 FLEXPART

FLEXPART-ECMWF modeling was used to explore the origin of air samples measured along the Polar 6 flight tracks. Figures 6 and 7 show the potential source regions of these air samples four days before the releases along the flight path. More specifically, the response function is shown to all releases of a passive tracer, which in this case has properties of dry air. If this response function would be folded with an emission flux of the tracer the concentration of this tracer at the release location along, the flight paths could be calculated. We chose to show the potential emission sensitivity after four days. Sharma et al., (1999) showed that atmospheric DMS(g) lifetime was 2.5 to 8 days in the high Arctic. More details about FLEXPART and the potential emissions sensitivity (PES) could be found in Stohl et al. (2005) and references therein.

Figure 6 shows two examples of FLEXPART-ECMWF PES for 4-day back trajectories in July 2014: an influence from a broad area and especially Lancaster Sound (local region) and north on July 12th (Figure 6, left panel), and Hudson Bay, and Baffin Bay (south) on July 19th (Figure 6, right panel). A more detailed analysis of PES reveals that the measured air mass descended from >1500 m on July 19th, which may explain the low DMS(g) mixing ratios.

Figure 7 shows some examples of FLEXPART-ECMWF PES simulations for 4-day back trajectories during April 2015. For the flights near Alert and Eureka on April 9 and 11, some DMS may have originated from ice-free areas of the Nares Strait and Baffin Bay (Figure 7, upper left and right panels, respectively). For the April 13 flight, the Norwegian Sea, North Atlantic Ocean and Hudson Bay are additional potential source regions (Figure 7, lower left panel). The highest DMS, measured on April 20 near Inuvik is associated with the North Pacific Ocean (Figure 7, lower right panel).

Assuming a DMS atmospheric lifetime of 1 to 4 days, these results suggest that the DMS(g) measured during July 2014 originated primarily from the local region over Baffin Bay and the Canadian Arctic Archipelago. For spring 2015, the DMS(g) sampled was from a range of sources, including Baffin Bay, possibly the Norwegian Sea, the North Atlantic Ocean and the North Pacific Ocean.

5 Conclusion

Atmospheric samples for DMS(g) measurements were collected at different altitudes aboard the Polar 6 aircraft expeditions during July 2014 and April 2015, as part of the NETCARE project. In this study, we present vertical profile measurements of DMS(g), together with model simulations to interpret these profiles. Vertical variations in DMS(g) mixing ratios are important since DMS(g) can influence aerosol concentrations via new particle formation and growth.

Our measured vertical profiles of DMS(g) suggest differences between the main sources and lifetime of DMS(g) during the Arctic summer and spring. For the summertime flights near Lancaster Sound, Nunavut, Canada, DMS(g) mixing ratios were higher near the surface (maximum > 110 pptv) and lower at higher altitudes up to 3 km. The highest mixing ratios were found above ice edges and open waters suggesting that the Arctic Ocean in the vicinity of the aircraft was the main source of DMS(g). Oxidation and/or limited vertical mixing could contribute to the decline of DMS(g) mixing ratios with altitude. During the springtime pan-Arctic flights from Svalbard to the Canadian Arctic Archipelago and ending near Inuvik, Northwest Territories, the measured DMS(g) mixing ratios were unusually high (> 100 pptv), and more uniform with altitude than during summer. DMS(g) mixing ratios in samples collected in the free troposphere (>2000 m) during April ranged from 60-134 pptv. Transport of DMS(g) to the high-Arctic from other regions of the Arctic and/or at lower latitudes and reduced oxidizing potential in springtime relative to summer may explain these observations.

The DMS(g) vertical profile along the flight tracks was simulated with the GEOS-Chem chemical transport model. The measurement and simulated co-sampled campaign-mean DMS(g) vertical profile agreed within a factor of 3 for both July 2014 and April 2015. A sensitivity test indicated that the oceans north of 66°N contributed about 97% and 90% of simulated DMS(g) at altitudes below 500 m at the measurement sampling times in July and April, respectively. For the April flights, about 60% of the simulated DMS at altitudes between 500-3000 m was attributed to water north of 66°N. Potential emission sensitivity from FLEXPART analysis for the aircraft tracks showed that local sources (Lancaster Sound and Baffin Bay) primarily contributed to air sampled during July 2014. On the other hand, LRT from the northern tip of Greenland of air that originated over the waters to the northwest of Greenland as well as the North Pacific Ocean were important contributors to air masses sampled during April 2015.

In short, this study suggests a dominant role of the Arctic Ocean for DMS(g) in the Arctic during summer, and a significant contribution from LRT to DMS(g) in spring.

Acknowledgments

This study was part of the NETCARE (Network on Climate and Aerosols: Addressing Key Uncertainties in Remote Canadian Environments, http://www.netcare-project.ca/) and was supported by funding from NSERC. The authors also would like to thank the crew of the Polar 6 and fellow scientists. Data is available by email request (alnorman@ucalgary.ca). The GEOS-Chem model is freely available for download from www.geos-chem.org.

References

Alexander, B., Park, R. J., Jacob, D. J., Li, Q., Yantosca, R. M., Savarino, J., Lee, C., and Thiemens, M.: Sulfate formation in sea-salt aerosols: constraints from oxygen isotopes, J. Geophys. Res.-Atmos., 110, D10307, doi:10.1029/2004JD005659, 2005.

Alexander, B., Park, R. J., Jacob, D. J., and Gong, S.: Transition metal-catalyzed oxidation of atmospheric sulfur: global implications for the sulfur budget, J. Geophys. Res.-Atmos., 114, D02309, doi:10.1029/2008JD010486, 2009.

Aliabadi, A. A. Staebler, R. M. de Grandpré, J. Zadra, A. Vaillancourt, P.: Comparison of Estimated Atmospheric Boundary Layer Mixing Height in the Arctic and Southern Great Plains under Statically Stable Conditions: Experimental and Numerical Aspects Atmosphere-Ocean, 54 (1), 60-74, doi: 10.1080/07055900.2015.1119100, 2016a.

Aliabadi, A. A. Staebler, R. M., Liu, M., Herber, A.: Characterization and Parametrization of Reynolds Stress and Turbulent Heat Flux in the Stably-Stratified Lower Arctic Troposphere Using Aircraft Measurements, Boundary-Layer Meteorology, 161(1): 99-126, doi: 10.1007/s10546-016-0164-7, 2016b.

Albrecht, B. A.: Aerosols, Cloud Microphysics, and Fractional Cloudiness, Science. 245 (4923): 1227–30, 1989.

Andreae, M. O., H. Berresheim, T. W. Andreae, M. A. Kritz, T. S. Bates, and J. T. Merrill,: Vertical distribution of dimethylsulfide, sulfur dioxide, aerosol ions, and radon over the northeast Pacific Ocean. Journal of Atmospheric Chemistry 6.1-2, 1988.

Andreae, M.O.: Ocean-atmosphere interactions in the global biogeochemical sulfur cycle. Marine Chemistry 30, 1-29, 1990.

Ayers, G.P., Cainey, J. M.: The CLAW hypothesis: a review of the major developments. Environmental Chemistry 4, 366-374, 2007.

Barrie, L. A., J. W. Bottenheim, R. C. Schnell, P. J. Crutzen, and R. A. Rasmussen.: Ozone destruction and photochemical reactions at polar sunrise in the lower Arctic atmosphere. Nature 334: 138-141, 1988.

Barnes, I., Hjorth, J., Mihalopoulos, N.: Dimethyl sulfide and dimethyl sulfoxide and their oxidation in the atmosphere. Chemical Reviews 106, 940-975, 2006.

Bates, T.S., Charlson, R.J., Gammon, R.H.: Evidence for climate role of marine biogenic sulphur. Nature 329, 319-321, 1987.

Bey, I., Jacob, D. J., Yantosca, R. M., Logan, J. A., Field, B. D., Fiore, A. M., Li, Q., Liu, H. Y., Mickley, L. J., and Schultz, M. G.: Global modeling of tropospheric chemistry with assimilated meteorology: Model description and evaluation, J. Geophys. Res., 106, 23073, doi:10.1029/2001JD000807, 2001.

Bourgain, P., J. C. Gascard, J. Shi, and J. Zhao: Large-scale temperature and salinity changes in the upper Canadian Basin of the Arctic Ocean at a time of a drastic Arctic Oscillation inversion, Ocean Science, 9, 2, 447–460, doi:10.5194/os-9-447-2013, 2013.

Breider, T. J., Mickley, L. J., Jacob, D. J., Wang, Q., Fisher, J. A., Chang, R. Y.-W., Alexander, B., (2014), Annual distributions and sources of Arctic aerosol components, aerosol optical depth, and aerosol absorption, J. Geophys. Res-Atmos., 119, 4107–4124, doi:10.1002/2013JD020996.

Brioude, J., Arnold, D., Stohl, A., Cassiani, M., Morton, D., Seibert, P., Angevine, W., Evan, S., Dingwell, A., Fast, J. D., Easter, R. C., Pisso, I., Burkhart, J., and Wotawa, G.: The La grangian particle dispersion model FLEXPART-WRF version 3.1, Geosci. Model Dev., 6, 1889–1904, doi:10.5194/gmd-6- 1889-2013, 2013.

Carslaw, K.S., Lee, L.A., Reddington, C.L., Pringle, K.J., Rap, A., Forster, P.M., Mann, G.W., Spracklen, D.V., Woodhouse, M.T., Regayre, L.A. and Pierce, J.R.: Large contribution of natural aerosols to uncertainty in indirect forcing. *Nature*, *503*(7474), pp.67-71, 2013.

Charlson, R.J., Lovelock, J.E., Andreae, M.O., Warren, S.G.: Oceanic phytoplankton, atmospheric sulphur, cloud albedo and climate. Nature 326, 655-661, 1987.

Chatfield, R. B., and P. J. Crutzen: Are there interactions of iodine and sulfur species in marine air photochemistry?, J. Geophys. Res., 95(D13), 22,319-22,341, 1990.

Chang, R. Y.-W., Sjostedt, S. J., Pierce, J. R., Papakyriakou, T. N., Scarratt, M. G., Michaud, S., Levasseur, M., Leaitch, W. R., and Abbatt, J. P. D.: Relating atmospheric and oceanic DMS levels to particle nucleation events in the Canadian Arctic, Journal of Geophysical Research, Res.-Atmos., 116, D00S03, doi:10.1029/2011JD015926, 2011.

Chen, Q., Geng, L., Schmidt, J. A., Xie, Z., Kang, H., Dachs, J., Cole-Dai, J., Schauer, A. J., Camp, M. G., and Alexander, B.: Isotopic constraints on the role of hypohalous acids in sulfate aerosol formation in the remote marine boundary layer, Atmos. Chem. Phys., 16, 11433-11450, doi:10.5194/acp-16-11433-2016, 2016.

Croft, B., Martin, R. V., Leaitch, W. R., Tunved, P., Breider, T. J., D'Andrea, S. D., and Pierce, J. R.: Processes controlling the annual cycle of Arctic aerosol number and size distributions, Atmos. Chem. Phys., 16, 3665-3682, doi:10.5194/acp-16-3665-2016, 2016a.

Croft, B., Wentworth, G.R., Martin, R.V., Leaitch, W.R., Murphy, J.G., Murphy, B.N., Kodros, J.K., Abbatt, J.P. and Pierce, J.R.: Contribution of Arctic seabird-colony ammonia to atmospheric particles and cloud-albedo radiative effect. Nature Communications, 7, 13444, 2016b.

DeMore, W. B., S. P. Sander, D. M. Golden, R. F. Hampson, M. J. Kurylo, C. J. Howard, A. R. Ravishankara, C. E. Kolb, and M. J. Molina: Chemical kinetics and photochemical data for use in stratospheric modeling, JPL Publ., 97-4, 1-278, 1997.

Fairlie, T. D., Jacob, D. J., and Park, R. J.: The impact of transpacific transport of mineral dust in the United States, Atmos. Environ., 41, 1251–1266, 2007.

Fairlie, T. D., Jacob, D. J., Dibb, J. E., Alexander, B., Avery, M. A., van Donkelaar, A., and Zhang, L.: Impact of mineral dust on nitrate, sulfate, and ozone in transpacific Asian pollution plumes, Atmos. Chem. Phys., 10, 3999–4012, doi:10.5194/acp-10-3999-2010, 2010.

Fountoukis, C. and Nenes, A.: ISORROPIA II: a computationally efficient thermodynamic equilibrium model for K^+–Ca^{2+}–Mg^{2+}–NH^+_4 –Na^+–SO_4^{2-} –NO_3^- –Cl^- –H_2O aerosols, Atmos. Chem. Phys., 7, 4639–4659, doi:10.5194/acp-7-4639-2007, 2007.

Ferek, R. J., P. V. Hobbs, L. F. Radke, J. A. Herring, W. T. Sturges, and G. F. Cota: Dimethyl sulfide in the Arctic atmosphere, J. Geophys. Res., 100(D12), 26093–26104, doi:10.1029/95JD02374, 1995.

Fisher, J. A., Jacob, D. J., Wang, Q., Bahreini, R., Carouge, C. C., Cubison, M. J., Dibb, J. E., Diehl, T., Jimenez, J., L., Leibensperger, E. M., Lu, Z., Meinders, M. B. J., Pye, H. O. T., Quinn, P. K., Sharma, S., Streets, D. G., van Donkelaar, A., and Yantosca, R. M.: Sources, distribution, and acidity of sulfate-ammonium aerosol in the Arctic in winter-spring, Atmos. Environ., 45, 7301–7318, doi:10.1016/j.atmosenv.2011.08.030, 2011.

Fisher, J. A., Jacob, D. J., Soerensen, A. L., Amos, H. M., Steven, A., and Sunderland, E. M.: Riverine source of Arctic Ocean mercury inferred from atmospheric observations, Nat. Geosci., 5, 499–504, 2012.

Galí, M., and R. Simó: Occurrence and cycling of dimethylated sulfur compounds in the Arctic during summer receding of the ice edge, Marine Chemistry, 122, 105–117, doi:10.1016/j.marchem.2010.07.003, 2010.

Ghahremaninezhad, R., Norman, A.-L., Abbatt, J. P. D., Levasseur, M., and Thomas, J. L.: Biogenic, anthropogenic and sea salt sulfate size-segregated aerosols in the Arctic summer, Atmos. Chem. Phys., 16, 5191-5202, doi:10.5194/acp-16-5191-2016, 2016.

Herrmann, H., Ervens, B., Jacobi, H. W., Wolke, R., Nowacki, P., Zellner, R.: CAPRAM2.3: A chemical aqueous phase radical mechanism for tropospheric chemistry. J. Atmos. Chem., 36, 231−284, 2000.

Hoffmann E. H., Tilgner A., Schrödner R., Bräuer P., Wolke R., and Herrmann H.: An advanced modeling study on the impacts and atmospheric implications of multiphase dimethyl sulfide chemistry, PNAS Early Edition, doi: 10.1073/pnas.1606320113, 2016.

IPCC, "Intergovernmental Panel on Climate Change", Christensen, J. H.: In Climate Change. The Physical Science Basis (eds Stocker, T. F. et al.) Ch. 14, IPCC, Cambridge Univ. Press, 2013.

Kulmala, M., Laakso, L., Lehtinen, K. E. J., Riipinen, I., Dal Maso, M., Anttila, T., Kerminen, V.-M., Hõrrak, U., Vana, M., and Tammet, H.: Initial steps of aerosol growth, Atmos. Chem. Phys., 4, 2553-2560, doi:10.5194/acp-4-2553-2004, 2004.

Kupiszewski, P., Leck, C., Tjernström, M., Sjogren, S., Sedlar, J., Graus, M., Müller, M., Brooks, B., Swietlicki, E., Norris, S., and Hansel, A.: Vertical profiling of aerosol particles and trace gases over the central Arctic Ocean during summer, Atmos. Chem. Phys., 13, 12405-12431, doi:10.5194/acp-13-12405-2013, 2013.

Lana, A., Bell, T. G., Simó, R., Vallina, S. M., Ballabrera-Poy, J., Kettle, A. J., Dachs, J., Bopp, L., Saltzman, E. S., Stefels, J., Johnson, J. E., and Liss, P. S.: An updated climatology of surface dimethlysulfide concentrations and emission fluxes in the global ocean, Global Biogeochem. Cy., 25, GB1004, doi:10.1029/2010GB003850, 2011.

Lathem, T. L., Beyersdorf, A. J., Thornhill, K. L., Winstead, E. L., Cubison, M. J., Hecobian, A., Jimenez, J. L., Weber, R. J., Anderson, B. E., and Nenes, A.: Analysis of CCN activity of Arctic aerosol and Canadian biomass burning during summer 2008, Atmos. Chem. Phys., 13, 2735-2756, doi:10.5194/acp-13-2735-2013, 2013.

Leaitch, W.R., S. Sharma, L. Huang, A. M. Macdonald, D. Toom-Sauntry, A. Chivulescu, K. von Salzen, J.R. Pierce, N.C. Shantz, A. Bertram, J. Schroder, A.-L. Norman, R.Y.-W. Chang: Dimethyl Sulphide Control of the Clean Summertime Arctic Aerosol and Cloud, Elementa: Science of the Anthropocene 1: 000017, doi: 10.12952/journal.elementa.000017, 2013.

Leaitch, W. R., Korolev, A., Aliabadi, A. A., Burkart, J., Willis, M., Abbatt, J. P. D., Bozem, H., Hoor, P., Köllner, F., Schneider, J., Herber, A., Konrad, C., and Brauner, R.: Effects of 20–100 nanometre particles on liquid clouds in the clean summertime Arctic, Atmos. Chem. Phys., 16, 11107-11124, doi:10.5194/acp-2015-999, 2016.

Leck, C., and E. K. Bigg: Biogenic particles in the surface microlayer and overlaying atmosphere in the central Arctic Ocean during summer, Tellus, Ser. B, 57,305–316, 2005.

Leck, C., and E. K. Bigg: Source and evolution of the marine aerosol - A new perspective, Geophysical Research Letters, 32, 1–4, 2005b.

Leck, C. and Persson, C.: The central Arctic Ocean as a source of dimethyl sulfide—seasonal variability in relation to biological activity. Tellus 48B, 156–177, 1996.

Levasseur, M.: Impact of Arctic meltdown on the microbial cycling of sulfur. Nature Geoscience, 6 (9): 691-700, 2013.

Li, S. M., L. A. Barrie, R. W. Talbot, R. C. Harriss, C. I. Davidson, and J. L. Jaffrezo: Seasonal and geographic variations of methanesulphonic acid in the Arctic troposphere, Atmos. Environ., 27, 3011 – 3024, 1993.

Liao, H., Henze, D. K., Seinfeld, J. H., Wu, S., and Mickley, L. J.: Biogenic secondary organic aerosol over the United States: comparison of climatological simulations with observations, J. Geophys. Res.-Atmos., 112, D06201, doi:10.1029/2006JD007813, 2007.

Liss, P. S. and Merlivat, L.: Air-sea gas exchange rates: introduction and synthesis, in: The Role of Air-Sea Exchange in Geochemical Cycling, Springer, 113–127, 1986.

Lunden, J., Svensson, G., Wisthaler, A., Tjernstrom, M., Hansel, A. and Leck, C.: The vertical distribution of atmospheric DMS in the high Arctic summer. Tellus B, 62: 160–171. doi: 10.1111/j.1600-0889.2010.00458, 2010.

Matrai, P. A. and Vernet, M.: Dynamics of the vernal bloom in the marginal ice zone of the Barents Sea: dimethyl sulfide and dimethylsulfoniopropionate budgets. Journal of Geophysical Research, 102(C10), 22 965–22 979, 1997.

Mungall, E. L., Croft, B., Lizotte, M., Thomas, J. L., Murphy, J. G., Levasseur, M., Martin, R. V., Wentzell, J. J. B., Liggio, J., and Abbatt, J. P. D.: Dimethyl sulfide in the summertime Arctic atmosphere: measurements and source sensitivity simulations, Atmos. Chem. Phys., 16, 6665-6680, doi:10.5194/acp-16-6665-2016, 2016.

Najafi M.R, Francis W. Zwiers, Nathan P. Gillett: Attribution of Arctic temperature change to greenhouse-gas and aerosol influences. Nature Climate Change 5, 246–249, 2015.

Park, R. J., Jacob, D. J., Chin, M., and Martin, R. V.: Sources of carbonaceous aerosols over the United States and implications for natural visibility, J. Geophys. Res.-Atmos., 108, 4355, doi:10.1029/2002JD003190, 2003.

Park, R. J., Jacob, D. J., Field, B. D., Yantosca, R. M., and Chin, M.: Natural and transboundary pollution influences on sulfate-nitrate-ammonium aerosols in the United States: implications for policy, J. Geophys. Res.-Atmos., 109, D15204, doi:10.1029/2003JD004473, 2004.

Park, R. J., Jacob, D. J., Kumar, N., and Yantosca, R. M.: Regional visibility statistics in the United States: natural and transboundary pollution influences, and implications for the Regional Haze Rule, Atmos. Environ., 40, 5405–5423, 2006.

Pierce, J. R., Evans, M. J., Scott, C. E., D'Andrea, S. D., Farmer, D. K., Swietlicki, E., and Spracklen, D. V.: Weak global sensitivity of cloud condensation nuclei and the aerosol indirect effect to Criegee + SO2 chemistry, Atmos. Chem. Phys., 13, 3163-3176, doi:10.5194/acp-13-3163-2013, 2013.

Quinn and T. S. Bates: The case against climate regulation via oceanic phytoplankton sulfur emissions. Nature 480, 51–56, doi:10.1038/nature 10580, 2011.

Rempillo, O., Seguin, A. M., Norman, A.-L., Scarratt, M., Michaud, S., Chang, R., Sjostedt, S., Abbatt, J., Else, B., Papakyriakou, T., Sharma, S., Grasby, S., and Levasseur, M.: Dimethyl sulfide air-sea fluxes and biogenic sulfur as a source of new aerosols in the Arctic fall, Journal of Geophysical Research, Atmosphere, 116, D00S04, doi:10.1029/2011JD016336, 2011.

Richards, S. R., Rudd, J. W. M., and Kelly, C. A.: Organic volatile sulfur in lakes ranging in sulfate and dissolved salt concentration over five orders of magnitude, Limnol. Oceanogr., 39, 562–572, doi:10.4319/lo.1994.39.3.0562, 1994.

Rotstayn, L., Lohmann, U.: Simulation of the tropospheric sulfur cycle in a global model with a physically based cloud scheme, Journal of Geophysical Research, Atmosphere, 107, 4592, 2002.

Sharma, S.: Fluxes of dimethyl sulphide from the lakes of the Canadian BorealS hieldt o the atmosphereM, .Sc. thesis,Y ork Univ., Toronto, Ont., Canada, 1997.

Sharma, S., L. A. Barrie, D. Plummer, J. C. McConnell, P. C. Brickell, M. Levasseur, M. Gosselin, and T. S. Bates: Flux estimation of oceanic dimethyl sulfide around North America, J. Geophys. Res., 104(D17), 21327–21342, 1999.

Sharma, S., E. Chan, M. Ishizawa, D. Toom-Sauntry, S. L. Gong, S. M. Li, W. R. Leaitch, A. Norman, P.K. Quinn, T.S. Bates, M. Levasseur, L.A. Barrie, W. Maenhaut: Influence of Transport and Ocean Ice

Extent on Biogenic Aerosol Sulfur in the Arctic Atmosphere. J. Geophys. Res. Atmospheres, 117, DOI: 10.1029/2011JD017074, 2012.

Shupe, M. D., Persson, P. O. G., Brooks, I. M., Tjernström, M., Sedlar, J., Mauritsen, T., Sjogren, S., and Leck, C.: Cloud and boundary layer interactions over the Arctic sea ice in late summer, Atmos. Chem. Phys., 13, 9379-9399, doi:10.5194/acp-13-9379-2013, 2013.

Simpson, I. J., Blake, N. J., Barletta, B., Diskin, G. S., Fuelberg, H. E., Gorham, K., Huey, L. G., Meinardi, S., Rowland, F. S., Vay, S. A., Weinheimer, A. J., Yang, M., and Blake, D. R.: Characterization of trace gases measured over Alberta oil sands mining operations: 76 speciated C_2–C_{10} volatile organic compounds (VOCs), CO_2, CH_4, CO, NO, NO_2, NO_y, O_3 and SO_2, Atmos. Chem. Phys., 10, 11931-11954, doi:10.5194/acp-10-11931-2010, 2010.

Skamarock, W. C., J. B. Klemp, J. Dudhia, D. O. Gill, D. M. Barker, W. Wang, and J. G. Powers, A description of the Advanced Research WRF Version 2. NCAR Tech Notes-468+STR, 2005.

Sofen, E., Alexander, B., Kunasek, S. A.: The impact of anthropogenic emissions on atmospheric sulfate production pathways, oxidants and ice core $\delta^{17}O$ (sulfate), Atmos. Chem. Phys, 11, 3565−3578, 2011.

Stohl, A., Forster, C., Frank, A., Seibert, P., and Wotawa, G.: Technical note: The Lagrangian particle dispersion model FLEXPART version 6.2, Atmos. Chem. Phys., 5, 2461–2474, doi:10.5194/acp-5-2461-2005, 2005.

Tjernström, M., Leck, C., Birch, C. E., Bottenheim, J. W., Brooks, B. J., Brooks, I. M., Bäcklin, L., Chang, R. Y.-W., de Leeuw, G., Di Liberto, L., de la Rosa, S., Granath, E., Graus, M., Hansel, A., Heintzenberg, J., Held, A., Hind, A., Johnston, P., Knulst, J., Martin, M., Matrai, P. A., Mauritsen, T., Müller, M., Norris, S. J., Orellana, M. V., Orsini, D. A., Paatero, J., Persson, P. O. G., Gao, Q., Rauschenberg, C., Ristovski, Z., Sedlar, J., Shupe, M. D., Sierau, B., Sirevaag, A., Sjogren, S., Stetzer, O., Swietlicki, E., Szczodrak, M., Vaatto vaara, P., Wahlberg, N., Westberg, M., and Wheeler, C. R.: The Arctic Summer Cloud Ocean Study (ASCOS): overview and experimental design, Atmos. Chem. Phys., 14, 2823–2869, 2014.

Tjernström, M., Leck, C., Persson, P. O. G., Jensen, M. L., Oncley, S. P., Targino, A.: The summertime Arctic atmosphere: meteorological measurements during the Arctic Ocean Experiment 2001 (AOE-2001), Bulletin of the American Meteorological Society, 85, 1305–1321, 2004.

Twomey, S.: Pollution and the planetary albedo. Atmos. Environ., 8, 1251-1256, 1974.

von Glasow, R., and P. J. Crutzen: Model study of multiphase DMS oxidation with a focus on halogens, Atmospheric Chemistry and Physics, 4, 589–608, 2004.

Wang, Q., Jacob, D. J., Fisher, J. A., Mao, J., Leibensperger, E. M., Carouge, C. C., Le Sager, P., Kondo, Y., Jimenez, J. L., Cubison, M. J., and Doherty, S. J.: Sources of carbonaceous aerosols and deposited black carbon in the Arctic in winter-spring: implications for radiative forcing, Atmos. Chem. Phys., 11, 12453– 12473, doi:10.5194/acp-11-12453-2011, 2011.

Wentworth, G. R., Murphy, J. G., Croft, B., Martin, R. V., Pierce, J. R., Côté, J.-S., Courchesne, I., Tremblay, J.-É., Gagnon, J., Thomas, J. L., Sharma, S., Toom-Sauntry, D., Chivulescu, A., Levasseur, M., and Abbatt, J. P. D.: Ammonia in the summertime Arctic marine boundary layer: sources, sinks, and implications, Atmos. Chem. Phys., 16, 1937-1953, doi:10.5194/acp-16-1937-2016, 2016.

Willis, M. D., Burkart, J., Thomas, J. L., Köllner, F., Schneider, J., Bozem, H., Hoor, P. M., Aliabadi, A. A., Schulz, H., Herber, A. B., Leaitch, W. R., and Abbatt, J. P. D.: Growth of nucleation mode particles in the summertime Arctic: a case study, Atmos. Chem. Phys., 16, 7663–7679, doi:10.5194/acp-16-7663-2016, 2016.

Woodhouse, M. T., Mann, G. W., Carslaw, K. S., and Boucher, O.: Sensitivity of cloud condensation nuclei to regional changes in dimethyl-sulphide emissions, Atmos. Chem. Phys., 13, 2723– 2733, doi:10.5194/acp-13-2723-2013, 2013.

Yin, F., Grosjean, D., Seinfeld, J.H.: Photooxidation of dimethyl sulfide and dimethyl disulfide. I.: mechanism development. Journal of Atmospheric Chemistry 11, 309-364, 1990.

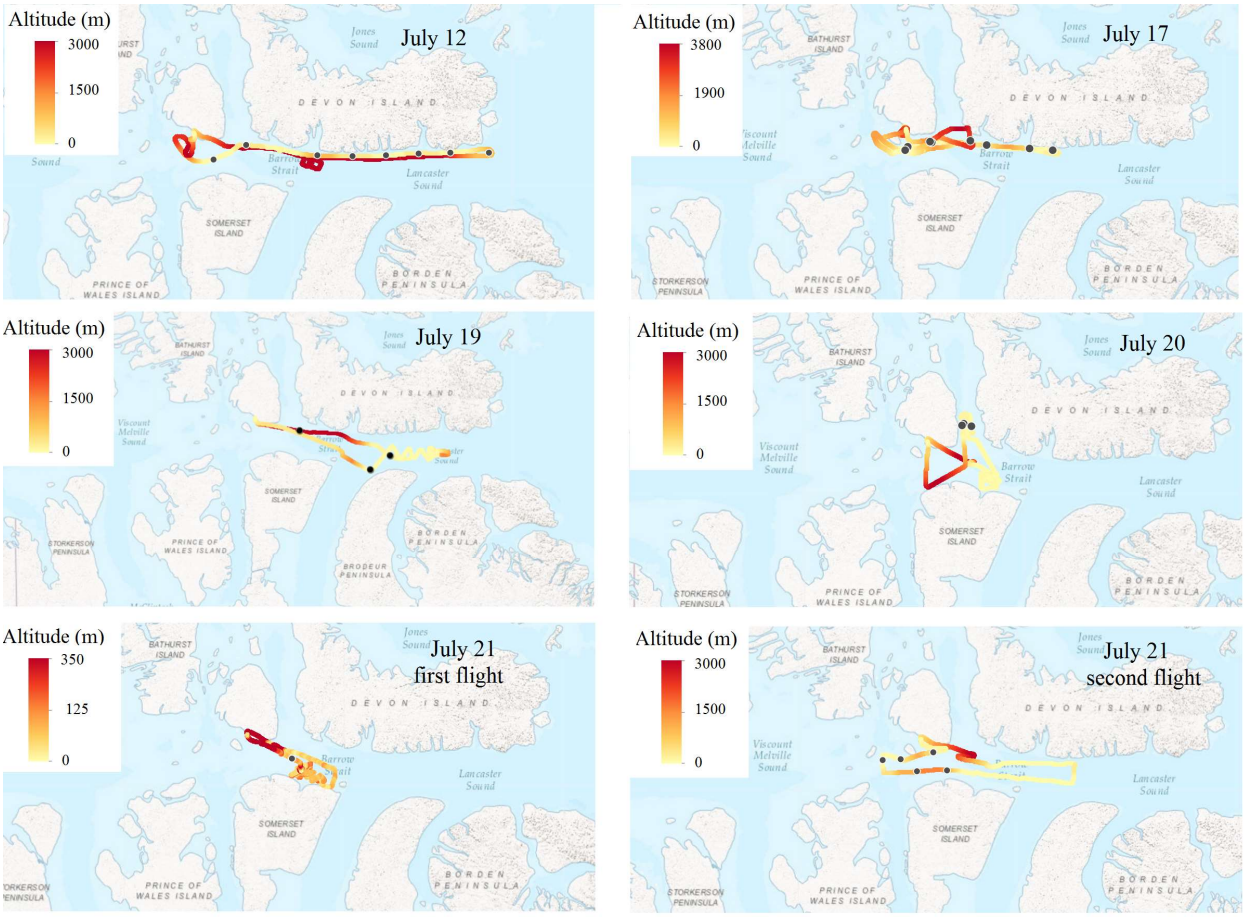

Figure 1. Polar 6 aircraft routes from 12 to 21 July 2014. Color bars indicate altitudes and sampling locations are shown with black dots.

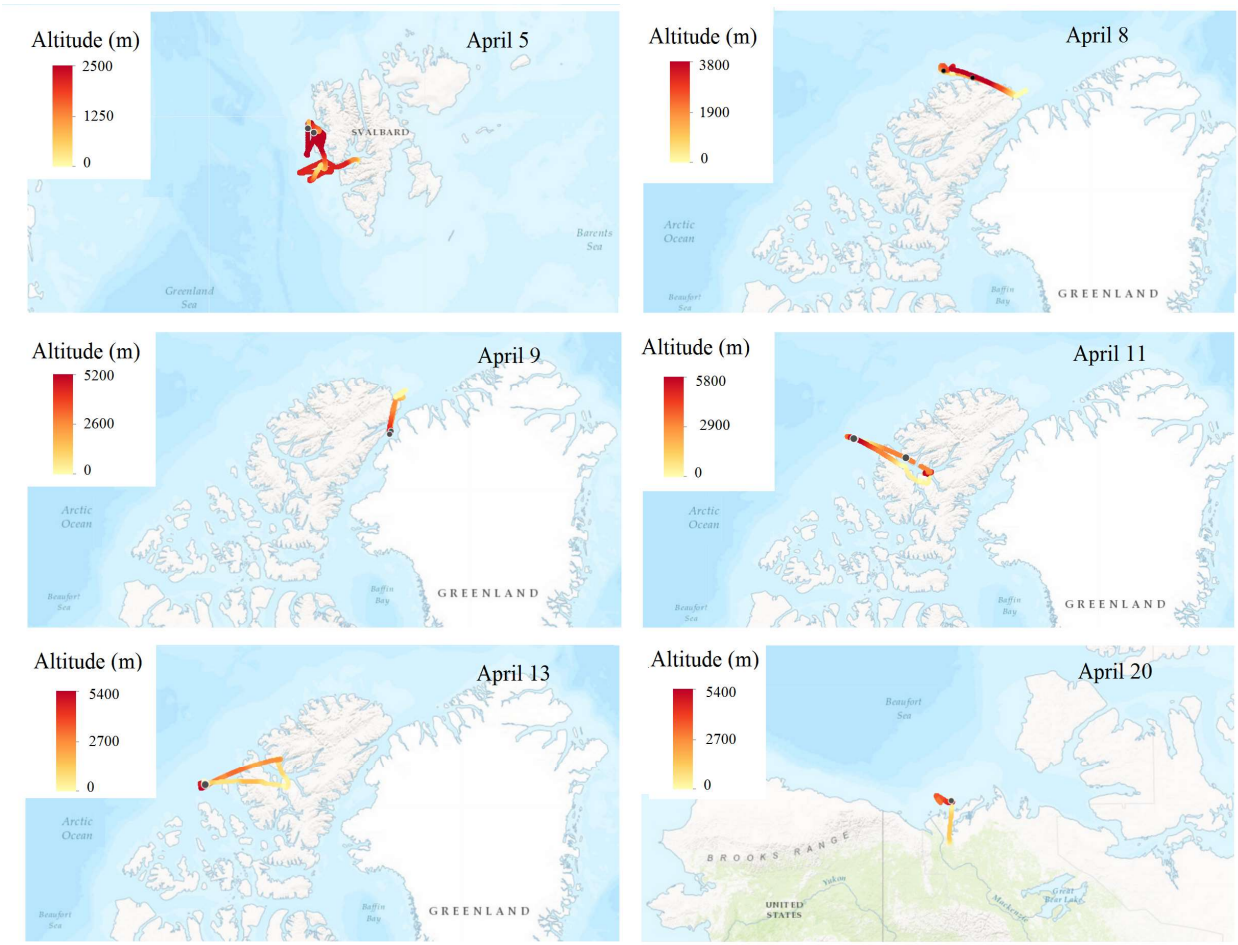

Figure 2. Polar 6 aircraft routes from 5 to 20 April 2015. Color bars indicate altitudes and sampling locations are shown with black dots.

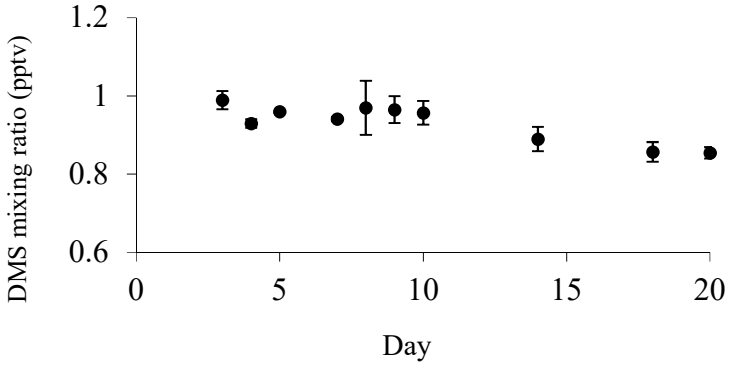

Figure 3. DMS mixing ratios versus Tenax storage days. Error bars indicate the standard deviation for each test.

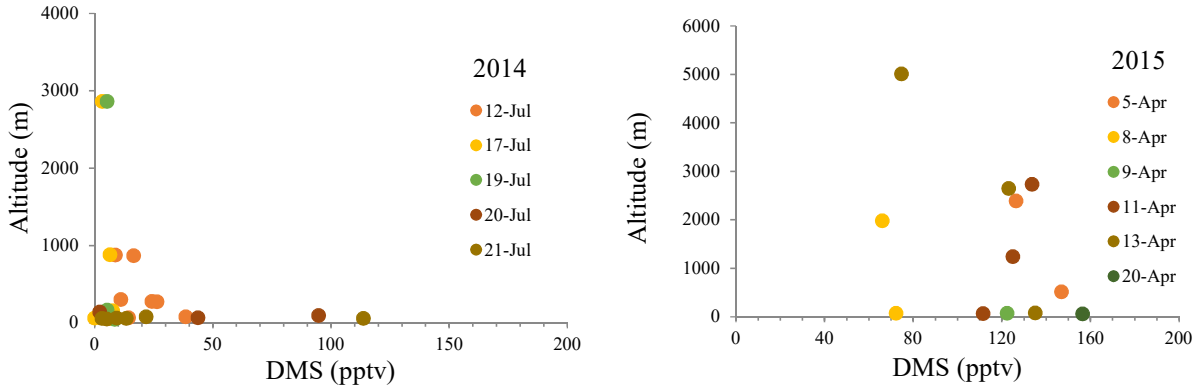

Figure 4. Sampling altitudes (m) versus DMS mixing ratios (pptv) for July 2014 (left panel) and April 2015 (right panel).

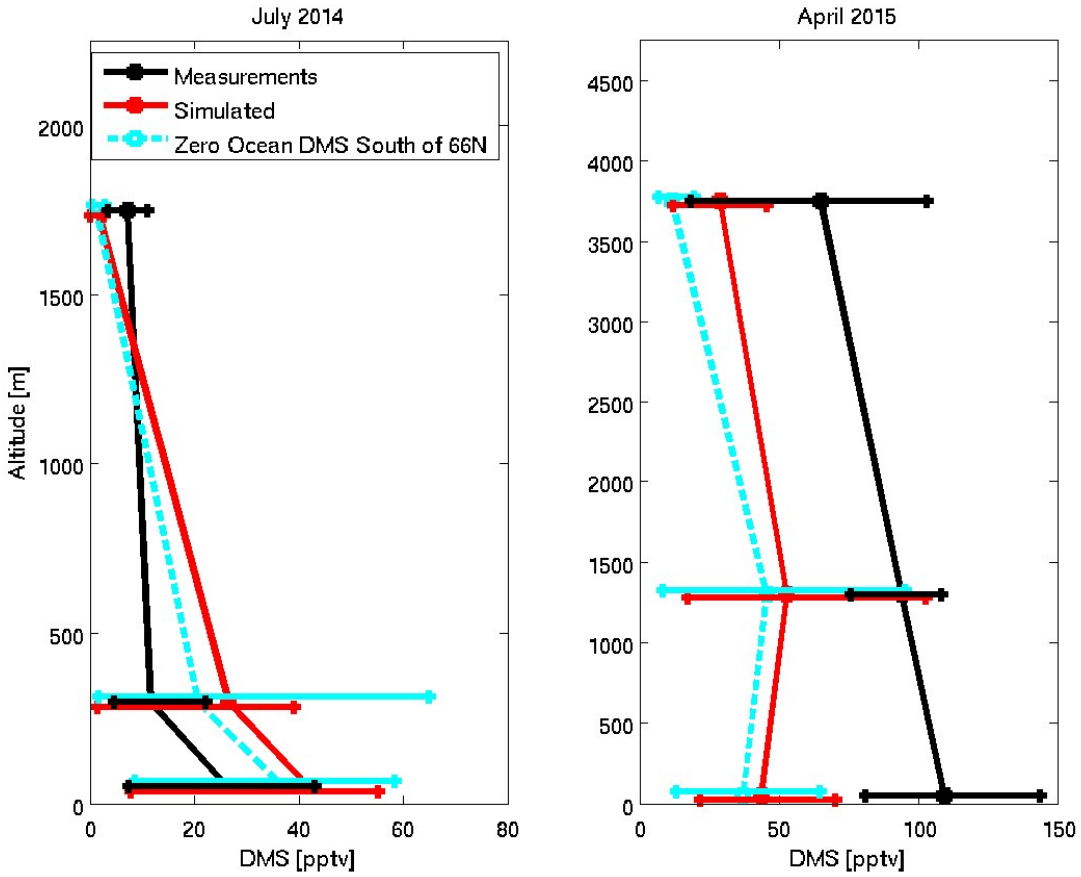

Figure 5. The campaign-mean vertical profile of DMS from the GEOS-Chem simulation (red line) and measurements (black line) for July 2014 and April 2015. Simulations for zero ocean DMS at latitudes south of 66°N (SimZeroBelow66) are shown as cyan dashed line. The 20th and 80th percentiles are shown by horizontal bars.

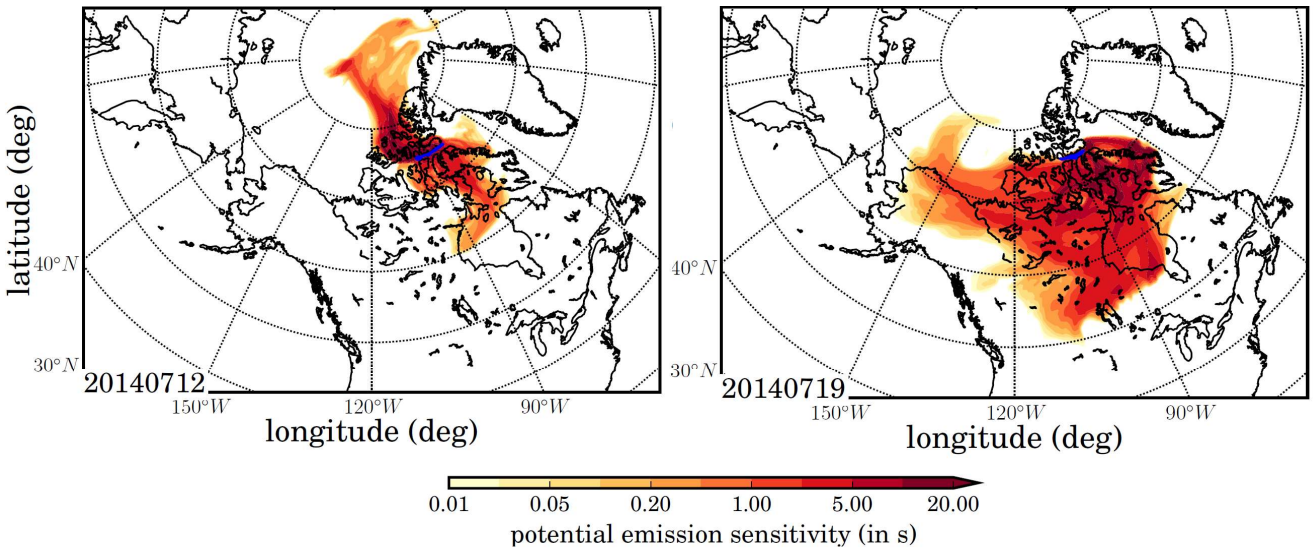

Figure 6. FLEXPART-ECMWF potential emissions sensitivity simulation plots for 4-day back trajectories for column from 0 to 1000 m on (a) July 12th (20:40:00 h UTC) and (b) July 19th (17:00:00 h UTC), 2014. The color bars indicate air mass residence time (seconds) before arriving at the aircraft location. The blue lines show Polar 6 aircraft routes.

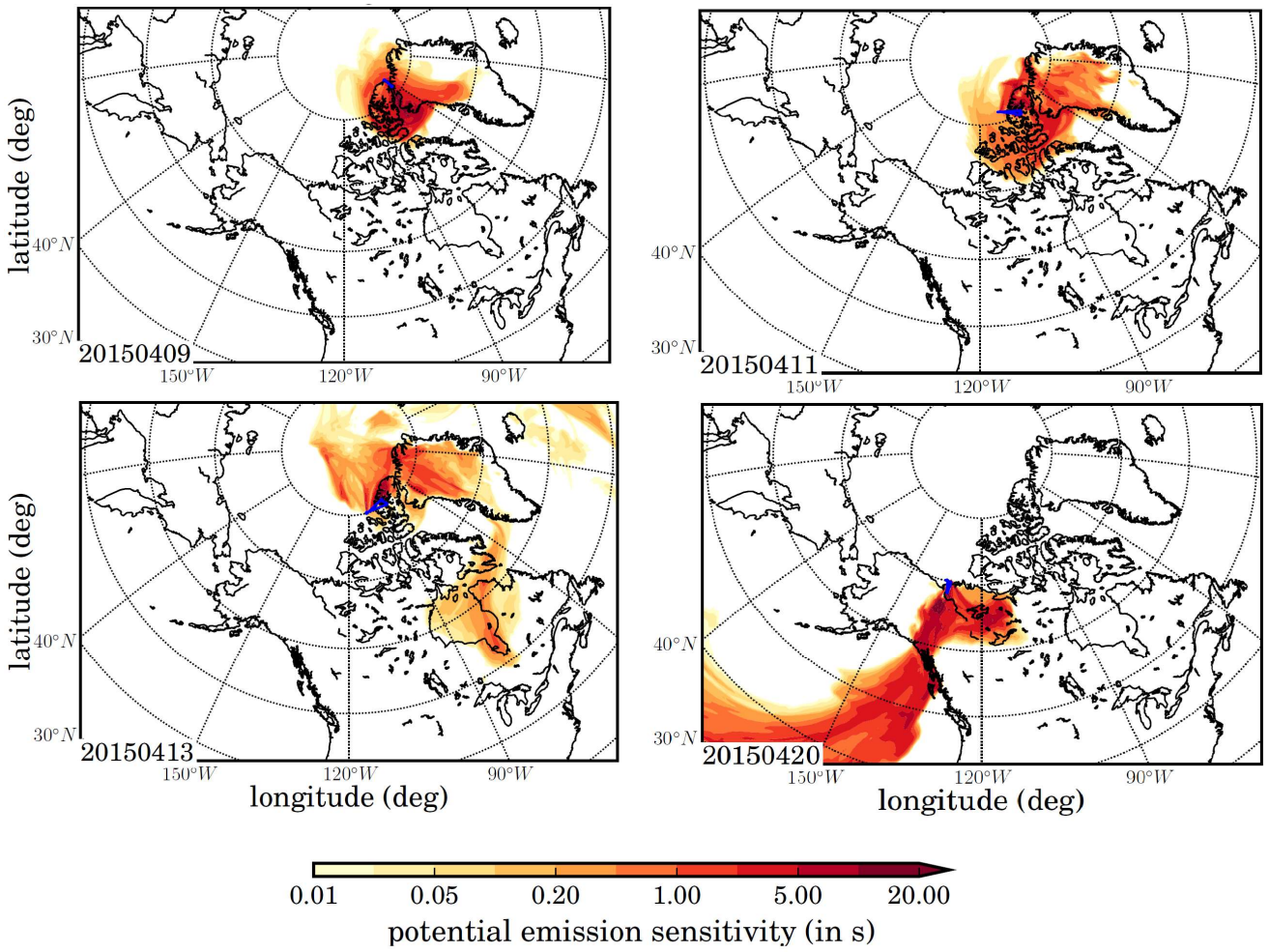

Figure 7. FLEXPART-ECMWF potential emissions sensitivity simulation plots for 4-day back trajectories for column from 0 to 1000 m on (a) April 9th (14:45:00 h UTC), (b) April 11th (18:55:00 h UTC), (c) April 13th (18:27:00 h UTC), and (d) April 20th (22:26:00 h UTC), 2015. The color bars indicate air mass residence time (seconds) before arriving at the aircraft location. The blue lines show Polar 6 aircraft routes.

Table 1. DMS mixing ratio values, sampling/analysis dates and sampling locations for July 2014 and April 2015.

Sample #	DMS (pptv)	Sampling Day	Analysis Day	Latitude (°)	Longitude (°)	Altitude (m)
1	17	12/07/2014	25/07/2014	74.45	-79.87	872
2	39	12/07/2014	25/07/2014	74.45	-81.85	78
3	26	12/07/2014	25/07/2014	74.44	-83.47	275
4	14	12/07/2014	25/07/2014	74.41	-85.11	69
5	24	12/07/2014	25/07/2014	74.40	-86.85	280
6	9	12/07/2014	25/07/2014	74.41	-88.63	880
7	11	12/07/2014	25/07/2014	74.55	-92.28	303
8	below detection	12/07/2014	25/07/2014	74.36	-93.97	57
9	below detection	17/07/2014	27/07/2014	74.47	-94.88	63
10	8	17/07/2014	27/07/2014	74.45	-88.64	159
11	8	17/07/2014	27/07/2014	74.42	-87.44	149
12	below detection	17/07/2014	27/07/2014	74.42	-95.01	58
13	below detection	17/07/2014	27/07/2014	74.54	-93.71	884
14	below detection	17/07/2014	27/07/2014	74.56	-91.66	2862
15	below detection	19/07/2014	27/07/2014	74.51	-92.20	2862
16	below detection	19/07/2014	27/07/2014	74.10	-86.53	165
17	9	19/07/2014	27/07/2014	73.86	-87.75	46
18	44	20/07/2014	25/07/2014	74.95	-93.09	67
19	below detection	20/07/2014	25/07/2014	74.92	-92.72	97
20	below detection	20/07/2014	25/07/2014	74.93	-93.18	143
21	22	21/07/2014	25/07/2014	74.39	-92.70	79
22	below detection	21/07/2014	25/07/2014	74.29	-93.62	51
23	below detection	21/07/2014	25/07/2014	74.28	-95.15	61
24	13	21/07/2014	25/07/2014	74.43	-96.91	61
25	114	21/07/2014	25/07/2014	74.45	-95.98	61
26	9	21/07/2014	25/07/2014	74.54	-94.35	65
27	127	05/04/2015	07/05/2015	78.91	10.31	2390
28	147	05/04/2015	07/05/2015	78.94	10.82	515
29	66	08/04/2015	07/05/2015	83.07	-71.99	1986
30	72	08/04/2015	07/05/2015	83.24	-78.59	76
31	122 ★	09/04/2015	07/05/2015	81.43	-63.39	78
32	134	11/04/2015	08/05/2015	80.77	-87.85	2733
33	112 ★	11/04/2015	08/05/2015	81.50	-99.72	68
34	125	11/04/2015	08/05/2015	81.57	-100.72	1244
35	75	13/04/2015	08/05/2015	80.06	-104.08	5015
36	123	13/04/2015	08/05/2015	80.09	-104.05	2651
37	135 ★	13/04/2015	08/05/2015	80.13	-103.95	79
38	157	20/04/2015	08/05/2015	70.00	-133.16	59

★ examples of DMS samples concurrent with ozone depletion events (<1 ppbv) during April.

Table 2. Simulated campaign-mean percent contribution of DMS from oceans north of 66°N to the GEOS-Chem simulated DMS at the sampling locations for the July 2014 and April 2015 flight tracks.

Altitude	July 2014	April 2015
0-100 m	98	88
100-500 m	97	90
500-3000 m	91	61

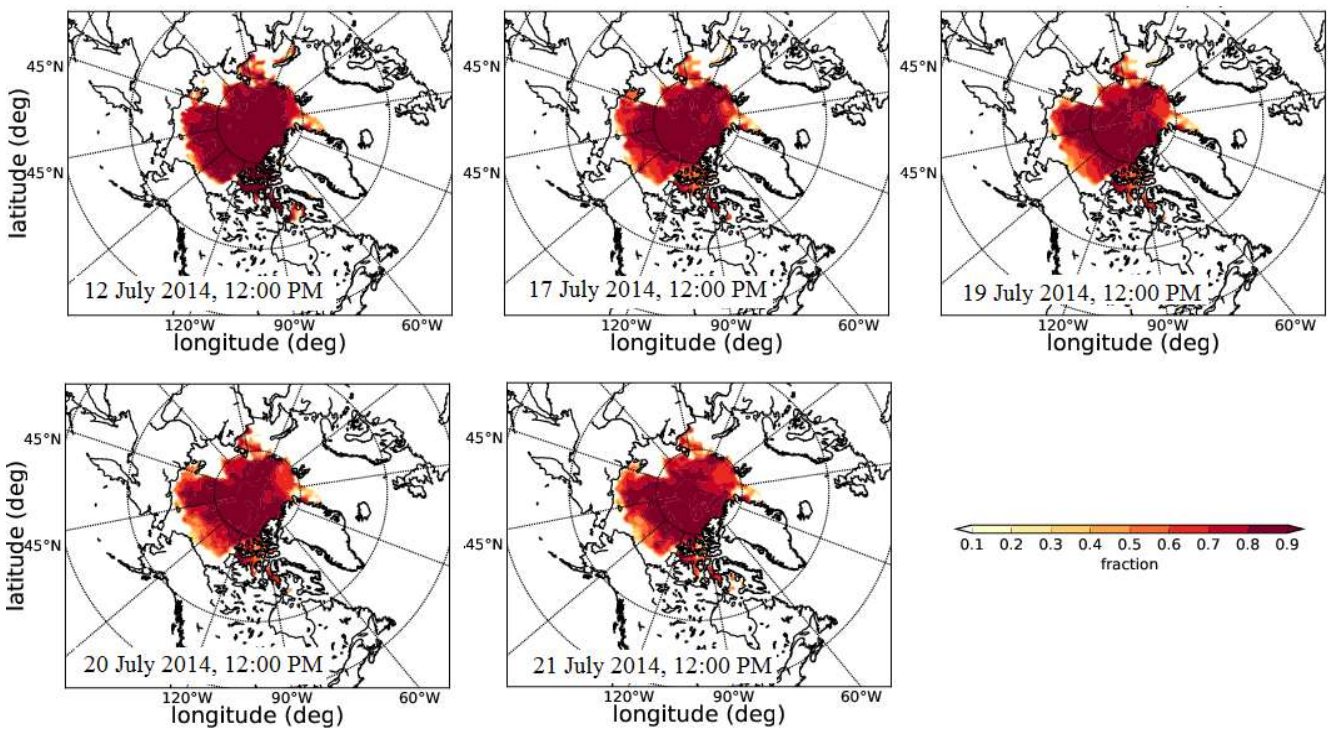

Figure S1. Distribution of the sea ice fraction over the Arctic for July 2014 flights. The fraction in each grid box specifies how much of the area was covered with sea ice. The data is taken from the operational analysis of the ECMWF model which is also used as meteorological input for the FLEXPART simulations.

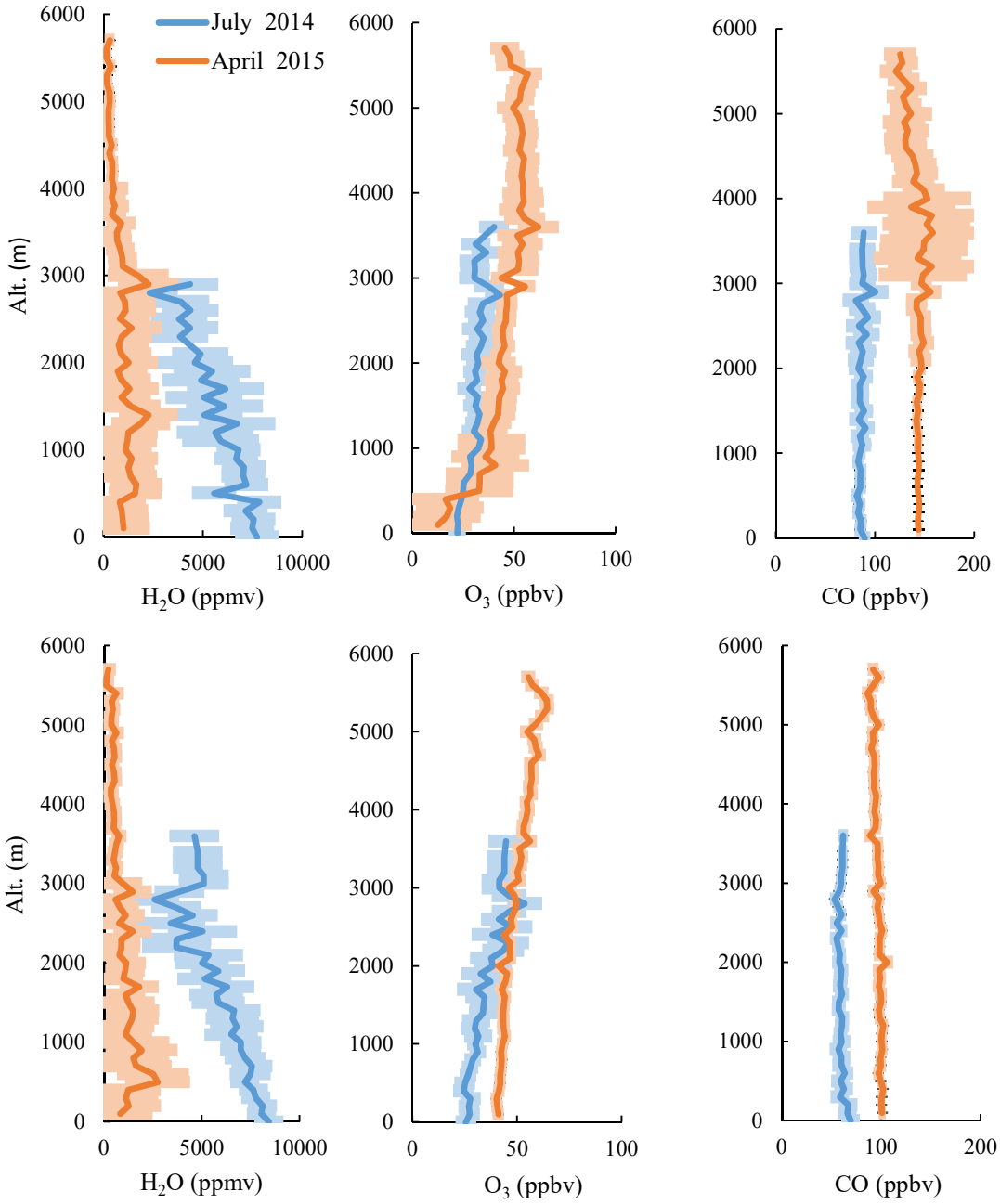

Figure S2. Average vertical profile of H_2O(g) and O_3 and CO during July 2014 (orange) and April 2015 (blue). Upper panels indicate and lower panels indicate measurements and GEOS-Chem results, respectively. Shadows show standard deviations.

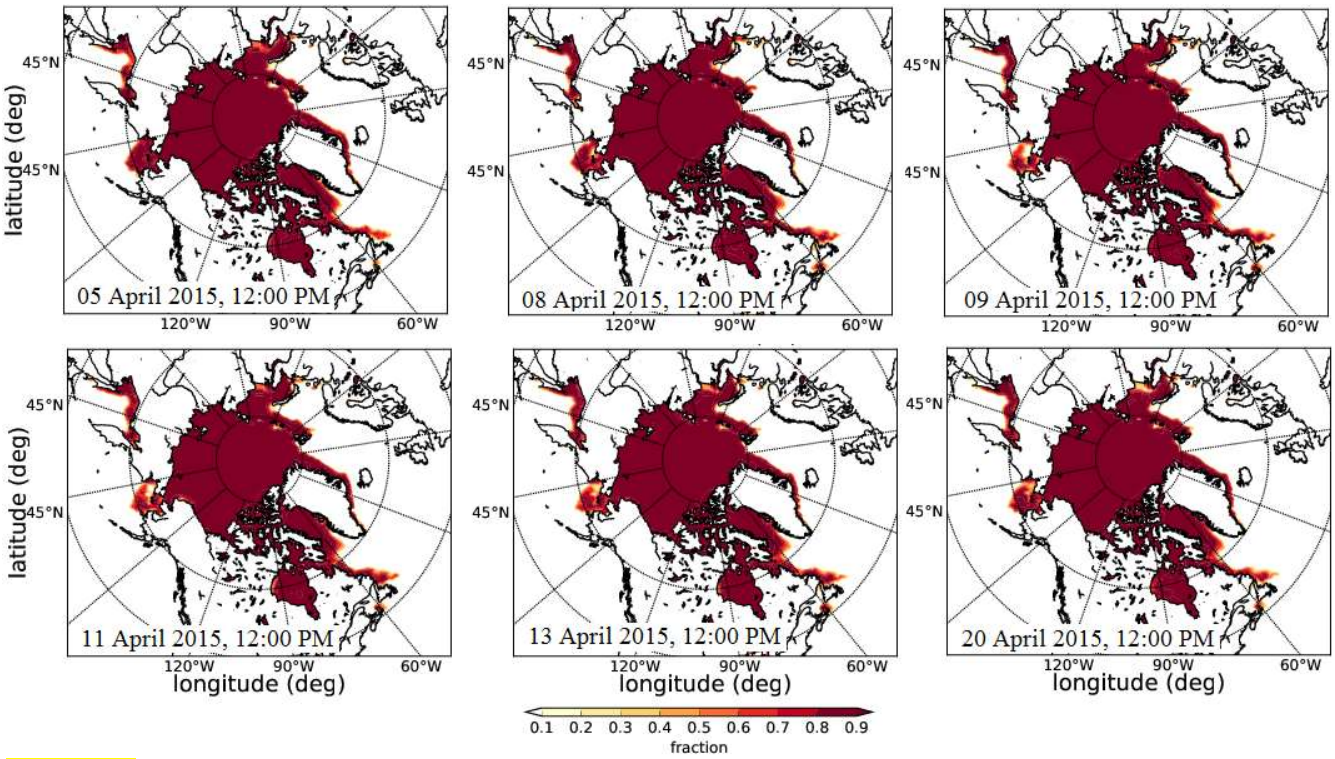

Figure S3. Distribution of the sea ice fraction over the Arctic for April 2015 flights. The fraction in each grid box specifies how much of the area was covered with sea ice. The data is taken from the operational analysis of the ECMWF model which is also used as meteorological input for the FLEXPART simulations.